On the Hydrogen Adsorption and Dissociation on Cu Surfaces and Nanorows

Leny Álvarez-Falcón, Francesc Viñes, Almudena Notario-Estévez, and Francesc Illas*

Departament de Química Física and Institut de Química Teòrica i Computacional (IQTCUB), Universitat de Barcelona, C. Martí i Franquès 1, 08028 Barcelona, Spain.

*Corresponding Author: francesc.illas@ub.edu

Abstract

Here we present a thorough density functional theory study, including and excluding dispersive forces interaction description, on the adsorption and dissociation of H_2 molecule on the low-index Miller Cu (111), (100), and (110) surfaces and two different surface Cu nanorows, all displaying a different number of surface nearest-neighbours, *nn*. The computational setup has been optimized granting an accuracy below 0.04 eV. Surface and nanorow energies —for which a new methodology to extract them is presented— are found to follow the *nn* number. However, the adsorption strength is found not to. Thus the adsorption energies seem to be governed by a particular orbital↔ band interaction rather than by the simple *nn* surface saturation. The van der Waals (*vdW*) forces are found to play a key role in the adsorption of H_2, and merely an energetic adjustment on chemisorbed H adatoms. No clear trends are observed for H_2 and H adsorption energies, and H_2 dissociation energy with respect *nn*, and no Brønsted-Evans-Polanyi, making H_2 adsorption and dissociation a trend outlier compared to other cases. H_2 is found to adsorb and dissociate on Cu(100) surface. On the Cu(111) surface the rather smaller H_2 adsorption energy would prevent H_2 dissociation, regardless is thermodynamically driven to. On Cu(110) surface the H_2 dissociation process would be endothermic, and achievable if adsorption energy is employed on surpassing the dissociation energy barrier. On low-coordinated sites on Cu nanorows, vdW plays a key role in the H_2 dissociation process, which otherwise is found to be endothermic. Indeed dispersive forces turn the process markedly exothermic. Nanoparticle Cu systems must display Cu(100) surfaces or facets in order to dissociate H_2, vital in many hydrogenation processes.

Keywords: Copper · Surfaces · Nanorows · Hydrogen Adsorption · Density Functional Calculations · Dispersive Forces.

1. Introduction

Hydrogen technology is a wide area of study, from its production to its use. As a reactant it is mainly used for crude oil refining into commercial liquid fuels, the production of high-value chemicals, and the evolving interest in using H_2 as a source of energy. Among the means of production the catalytic conversions are very important; such as the Steam Reforming (*SR*), the Partial Oxidation (*PO*), the Oxidative Steam Reforming (*OSR*), the Gasification of Carbon (*GC*), the carbon formation, and the Water Gas Shift reaction (*WGS*) [1]. In the case of SR and GC reactions, they may produce the same amount of CO_2 like in the regular fuel combustion, although the carbon dioxide can be removed from the product stream sequestered. These two reactions create the so-called *syngas* (a mixture primarily composed of CO and H_2), where CO can be used as a reactant in the WGS to produce more hydrogen [2].

In the case of methanol-reforming processes used to produce H_2 one can mention the Methanol Decomposition (*MD*), the Methanol Partial Oxidation (*MPO*), the Methanol Steam Reforming (*MSR*), and the Oxidative MSR (OMSR). In all these cases the Cu-based catalysts have been identified as outstandingly cost-effective for many reactions [3]. A number of recent studies assumed that copper and zirconia behaved in a bifunctional manner during the MD or methanol synthesis, with Cu serving as a site for the dissociation or removal of hydrogen molecules, and zirconia being an adsorption site for carbon-containing intermediates [4,5]. Similarly, for the WGS reaction Cu-based catalysts are widely employed and studied in order to elucidate the mechanism and the responsible sites of the catalytic activity [6].

As it can be seen the interaction of hydrogen molecules with metallic surfaces in general, of Copper in particular, is important for technological purposes and for modeling reactions taking place on solid surfaces [7]. The interaction of hydrogen with transition metal surfaces is a topic of considerable experiments and theoretical calculations, as they are used often to catalyze chemical reactions of industrial interest [8]. The prediction of the elementary processes occurring when H_2 is scattered on a metal surface is one of the main challenges in the field of heterogeneous catalysis [9]. As an example, the active sites for the H_2 production from the methanol reforming are still controversial [3]. For example dehydrogenation of cyclohexanol to cyclohexanone where Cu-based catalysts are the matter of investigations to understand the mechanism and active sites for the dehydrogenation process [10]. For these reasons hydrogen interaction and dissociation on the Cu(111) surface has turned out to became a

benchmark for understanding the reaction path. Nevertheless, metal nanoparticles exhibit a variety of facets, edges, and corner sites with different degrees of coordination, which can be crucial for the catalytic and synthesis purposes [11-14]. The understanding of the microscopic factors determining the reactivity of metal surfaces is of paramount interest since it might lead to the improvement of catalysts in a systematic way [15].

To contribute to the better understanding of the interaction of H_2 with different types of Cu surfaces, here we report a systematic theoretical study of the adsorbed and dissociated situations of molecular hydrogen on a variety of well-defined surface models. Moreover two types of Cu nanorows have been studied as approximations of less saturated sites. We considered lowest-index Miller Cu surfaces; (100), (110), (111), and two nanorows over the (111) surface, which altogether display a significant variety of low-coordination sites. In addition we explored the effect of vdW on such reaction on the given supports. With all this we discuss on the main aspects to consider when designing a Cu based catalyst for H_2 dissociation production and the effect of surface coordination in H_2 attachment and dissociation.

2. Theoretical Models and Computational Details

In this work Density Functional (*DF*) theory calculations have been carried out using the Perdew-Burke-Ernzerhof (*PBE*) exchange-correlation (*xc*) functional [16], within the Generalized Gradient Approximation (*GGA*). This xc functional has been found to be the best choice for simulating transition metals compared to other functionals within GGA or other approximations [17]. For the simulation of Cu bulk and surfaces the periodic VASP computation package was employed [18,19]. During the optimizations an electronic step convergence criterion of 10^{-6} eV has been used, together with a tight atomic force threshold of 0.001 eV/Å. Projector augmented wave pseudopotentials were used to treat the core electrons effect on valence electrons [20]. A plane-wave basis set has been used with a kinetic energy limit and a Monkhorst-Pack **k**-points mesh to sample the Brillouin zone [21]. These variables were optimized for bulk Cu sampling ranges of 250-600 eV and N×N×N (N=1-17), respectively. An optimal cut-off kinetic energy of 525 eV and a Monkhorst-Pack **k**-point mesh of 9×9×9 dimensions yielded variations in the total energy below 0.01 kJ mol^{-1} per bulk Cu atom by using slightly smaller kinetic energy limit and **k**-point mesh; consequently, these values have been used throughout the study. The calculated bulk Cu unit cell parameter, cohesive energy, and bulk modulus of 3.64 Å, 3.49 eV $atom^{-1}$, and 134 GPa,

respectively, obtained through a procedure described elsewhere [22], are in excellent agreement with the experimental values of 3.63 Å, 3.48 eV atom^{-1}, and 133 GPa, respectively, and also in excellent agreement with previous calculations [22], thus validating the present calculation setup.

To simulate the (100), (110), and (111) Cu surfaces, see Figure 1 for a depiction, a set of slab models were constructed using (1×1) supercells with increasing number of layers N_l (N_l = 1-15), but always keeping a vacuum region of 10 Å in the direction normal to the surface to avoid interaction between translationally repeated slabs. Bulk truncated, γ^{fix}, and relaxed, γ^{rel}, surface energies were computed following a procedure described elsewhere [23]. It has been found that a general thickness of N_l = 7 layers is enough to grant variations on any of the computed surface energies below 0.04 eV atom^{-1}. Final values are listed in Table 1; from them it is clear that the relaxation energy, ε^{rel}, defined as

$$\varepsilon^{rel} = \gamma^{fix} - \gamma^{rel} \quad (1),$$

is rather small, yet dependent on the stability of the surface; this is, most stable (111) surface features the smallest relaxation energy, and least stable (110) surface the largest one. Thus, the relaxation energy is in line with the degree of compactness of the surface, *i.e.* the larger the value of nearest-neighbors, *nn*, is, the lesser the relaxation energy. Already at this level one would expect surfaces with larger surface energies to be more active towards the attachment of adsorbates, as found previously in the literature [24].

Surface	(110)	(100)	(111)
γ^{fix} / J m^{-2}	1.601	1.515	1.313
γ^{rel} / J m^{-2}	1.548	1.500	1.307
ε^{rel} / J m^{-2}	0.053	0.015	0.006
nn	7	8	9

Table 1. Fixed and relaxed surface energies, γ^{fix} and γ^{rel}, respectively, as well as the relaxation energy, ε^{rel}, for the (100), (110), and (111) Cu surfaces, together with the number of nearest-neighbours for a surface Cu atom, *nn*.

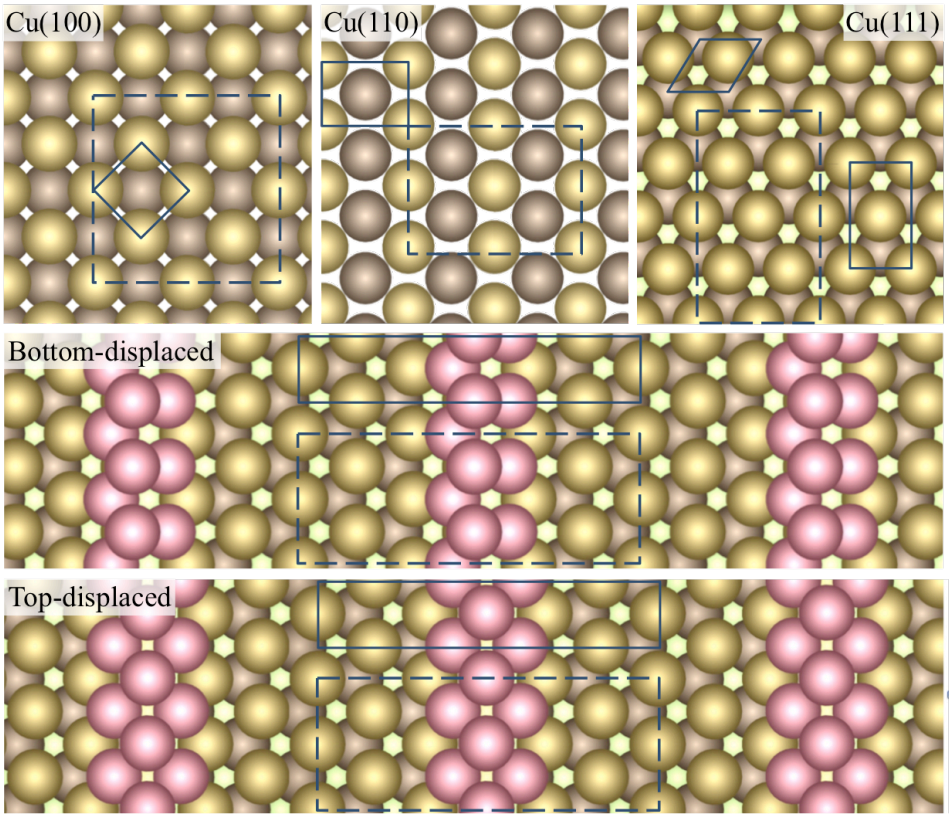

Figure 1. Top views of the studied Cu surfaces and nanorows. Spheres represent Cu positions, and color the height. The nanorows are shown in pink and decreasing the height it is shown gold, brown, and light green. Dashed lines denote the employed supercells and the solid lines denote the surface unit cells.

Once regular surfaces were duly well-described, we decided to expand our study to other periodic systems containing even less saturated Cu surface atoms. To do so, we decided to model Cu nanorows on the Cu(111) surface as recently similarly carried out for Au [25,26]. These nanorows were constructed starting from a symmetric relaxed Cu(111) surface of 7 layers, but building up a (1×3) supercell out of the (1×1) orthorhombic unit cell, as depicted in Figure 1. Six different arrangements were tested for the nanorow; in two of them all the three atoms conforming a section of the Cu nanorow are in line perpendicular to the direction of the nanorow (*in-line*), in which one case the bottom Cu atoms lay on hollow sites, (*in-line-hollow*) and in the other case on top positions (*in-line-top*). Two other cases are variations of the *in-line* but with the nanorow top Cu atom displaced (*displaced*), resulting in the *top-displaced-top* and *top-displaced-hollow* situations. Finally, the other two structures are equivalent to the *in-*

line ones but with one nanorow bottom Cu atom displaced (*bottom-displaced-hollow* and *bottom-displaced-top*).

However, geometry optimizations of the nanorows delivered that most of them either are high in energy or evolve to one of the two most stable ones, the so-called *bottom-displaced-hollow* and *top-displaced-hollow*, hereafter referred as to *bottom-* and *top-displaced*, respectively, for the sake of simplicity. Indeed, *bottom-displaced-top* was just 0.06 eV higher in energy than the *-hollow* counterpart, but since only one model with this particular coordination was needed, we chose the *-hollow* one for the rest of the study. As nanorows could be considered line defects, we chose to study their stability by calculating their absolute row energy, in a similar fashion as earlier performed to obtain absolute surface step energies [27]. According to it, the total energy of the slab, E, would be decomposed in the following terms

$$E = \varepsilon N + 2\gamma^{rel}(L \cdot W) + 2\beta W \qquad (2),$$

where ε is the energy of a bulk Cu atom, N the number of Cu atoms in the slab model, γ^{rel} the relaxed surface energy of the exposed (111) surface, and β the line energy of the Cu nanorow. Note that surface energies depend on the area exposed ($L \cdot W$) and nanorow line energies on the width of the slab (W), illustrated in Figure 3.

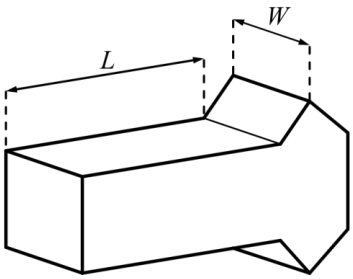

Figure 2. Sketch of a nanorow slab model, as well as the L and W geometric parameters used in equation 2.

The computed nanorow line energies for the *top-displaced*, and *bottom-displaced* nanorows are 8.27, and 7.77 eV nm^{-1}, respectively —equivalent to 2.260 and 2.782 J m^{-2}, respectively, given that nanorows occupy a certain Cu(111) surface area. The *top-displaced* arrangement seems to allow a better coupling of the nanorow Cu orbitals with the Cu(111) surface, being nanorow Cu bottom atoms bridging two Cu atoms of what it would be the Cu(111) surface. In the case of *bottom-displaced*, this

factor seems to be added to the point that every second bottom Cu atom is sitting on a Cu(111) surface hollow site, indeed, that which would be occupied for an ideal eighth Cu layer, fact that seems to add more stability to the system. In summary, both displaced situations have been further considered for the H_2 adsorption study. The *nn* of *top-* and *bottom-displaced* situations is 6 and 5, respectively. Note that, considering the equivalent surface energies of the nanorows, the stability seems to be highly governed by the number of nearest neighbors.

The hydrogen molecule adsorption on the different Cu surfaces and two different nanorows has been studied using supercells: on (100) and (110) surfaces a (2×2) supercell —56 and 28 Cu atoms, respectively—, in the case of the (111) surface a (2×2) supercell from the orthorhombic surface unit cell —56 Cu atoms—, and (2×3) supercells for the two studied nanorows —96 Cu atoms each—. In all cases for all the H_2 adsorption tested positions the molecule is placed at a 3 Å initial distance from the tested site, being the initial H-H bond length 0.75 Å. The molecule and the three top layers are relaxed during the calculations, allowing the system to reach a minimum energy. For these optimized structures, the adsorption energy has been calculated with the following equation:

$$E_{ads} = E_{H_2/surf} - E_{surf} - E_{H_2} \quad (3),$$

where E_{ads} is the adsorption energy, $E_{H_2/surf}$ is the energy of the hydrogen molecule interacting with the metallic surface, and E_{surf} and E_{H_2} are the energies of the pristine surface and of the isolated molecule, respectively. The isolated molecule has been optimized using the same setup but isolating it within an asymmetric cell of 9×10×11 Å dimensions, and carrying out the calculations at the **Γ** point. Within this definition, adsorption energy values are negative, and so the more negative the E_{ads} value, the stronger the interaction. Note by passing by that interaction among translationally repeated H_2 molecules when adsorbed, and the changes by including a different **k**-point set are minimal, below 0.01 kJ mol^{-1}. Those preferred sites, whose population is above 1% according to a Gibbs distribution at 300 K, have been re-optimized considering a description of the dispersive forces following the dispersion correction D2 of Grimme [28], and adsorption energies have been calculated likewise. This dispersion correction has been previously found to be appropriate to describe the adsorption of molecules on Cu substrates [29], and also on the interaction of graphene on metal surfaces [30]. Note

in passing by that similar correction D3 of Grimme [31] was found to correctly describe the H_2 adsorption, yet there on oxide clusters [32].

The final H_2 dissociation situation, i.e. two H adatoms on the Cu systems, has been studied similarly yet deliberately placing the H atoms in nearby positions according to earlier extensive experimental and theoretical works, which show that H adatoms prefer to sit on face-centered cubic (*fcc*) hollow sites and four-fold hollow sites on Cu(111) and Cu(100) surfaces, respectively [33-35], and over short-bridges (*sb*) and long-bridges (*lb*) of Cu(110) surfaces [35]. In the case of Cu nanorows, they display small (111) or (100) like facets. Thus, the two H atoms have been placed on hollow positions of nanorow adjacent facets. Charges on atoms have been estimated through a Bader analysis of the electron density [36], yet in all the studied cases charge transfer from Cu substrate to/from hydrogen species has been found to be essentially zero, this is, they are in all the studied cases neutral species, and so this aspect is no longer referred in the oncoming discussion.

The H_2 dissociation path connecting H_2 and 2 H adatoms has been studied obtaining the Transition State (*TS*) structures using the dimer approach [37], at the PBE-D2 level. The gained TS have been characterized by a vibrational frequency analysis, performed by the construction and diagonalization of the Hessian matrix by finite displacements of 0.03 Å. The TSs featured only an imaginary frequency in all the cases. Then, the H_2 dissociation energy barrier, E_{barr}, is calculated as:

$$E_{barr} = E_{TS} - E_{H_2/surf} \quad (4),$$

where E_{TS} is the total energy of the located TS. Thus, energy barriers are delivered positive.

3. Results and Discussion

3.1. H_2 Adsorption

Let us being with the H_2 molecule adsorption process. For it, aside from the adsorption energy values, E_{ads}, we provide general features for the final optimized configurations: the shortest distance between one H atom of the H_2 molecule and a substrate Cu atom, *d*, the H-H bond length, *l*, and the angle between the surface and the H_2 bond, α, i.e. the angle that the line connecting both H atoms in H_2, extrapolated to contact the surface, forms with respect the surface plane. In this sense, an angle of 0º implies H_2 molecule planar to the surface, whereas 90º implies H2 molecule perpendicular to the surface.

3.1.1. *H_2 Adsorption on Cu(111)*

We start from most compact Cu surface, the (111). Here five highly symmetric adsorption geometries on the Cu(111) surface were sampled, whose Initial Configuration (*IC*) and Final Configuration (*FC*) are shown in Figure 3. These include top (1) and bridge sites (2a and 2b), one hexagonal close-packed (*hcp*) hollow site (3a) and one fcc hollow site (3b). Energetic and geometric information are encompassed in Table 2. The highest stability of Cu(111) surface, as shown in Table 1, is translated into extremely weak adsorption energies, where all sites feature the same E_{ads} values. Indeed, the Cu surface repulsion normally makes the molecule rotate to adopt a perpendicular direction, see angles α on Table 2, with the caveat of 2a position. Here no site seems to be especially active in elongating H_2 bond length, nor one implies a special attraction to the surface. Indeed, PBE results show that H_2 molecule is merely physisorbed, floating over the Cu(111) surface. However, when D2 dispersive forces correction is applied, H_2 molecules approach the Cu(111) surface by ~0.9 Å, despite the H_2 interatomic distance is unperturbed. Moreover, the adsorption energy is increased manifold, but still being rather low, to values of *circa* -0.08 eV. Note that the addition of dispersive forces does not allow discriminating in between the sampled adsorption sites. Thus, one can state that H_2 adsorption on Cu(111) surface is governed by van der Waals (*vdW*) interactions, but equally for all the adsorption configurations.

Recent calculations showed the perpendicular disposition of H_2 on Cu(111) surface —as well as on Ni(111) [38]. However no preferential adsorption site was reported, although it was stated that *fcc* and *hcp* hollow sites were somewhat more stable, as here found. In the case of atomic H, *fcc* seems to be slightly more stable, as also found on an ammonia decomposition study [39], where the perpendicular disposition of H_2 —here over a top site— was reported at standard DF level with no vdW description. Finally, note that many of the experimental mechanisms proposed for WGS, SR, or MD reactions on Cu(111) imply that the H_2 generation step goes directly from the atomic H combination to H_2 in the gas phase [4-6], pointing for a very low adsorption energy of H_2, and thus, a solid statement insomuch that H_2 is weakly physisorbed. However, over different Cu surfaces the H_2 interactions may change, as is discussed in the next sections.

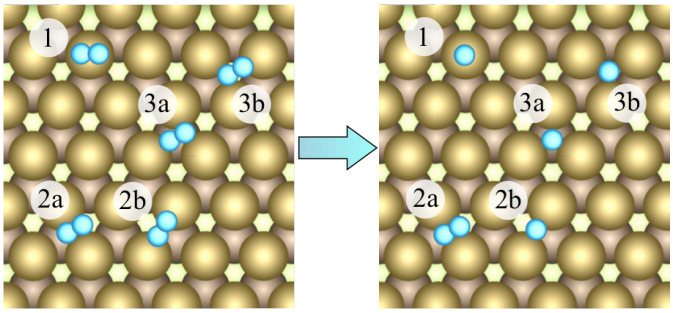

Figure 3. IC (left) and FC (right) for the sampled H_2 adsorption high-symmetry sites on Cu(111) surface. H atoms are light blue spheres, while the rest of color-coding is as in Figure 1.

		1a	2a	2b	3a	3b
PBE	***l* / Å**	0.75	0.75	0.75	0.75	0.75
	***d* / Å**	3.44	3.71	3.39	3.38	3.44
	α / º	88.1	1.1	88.3	86.8	89.3
	E_{ads} **/ eV**	-0.001	-0.001	-0.002	-0.001	-0.001
PBE-D2	***l* / Å**	0.76	0.75	0.75	0.75	0.75
	***d* / Å**	2.51	3.15	2.52	2.47	2.48
	α / º	85.3	2.1	88.4	88.7	89.3
	E_{ads} **/ eV**	-0.07	-0.07	-0.07	-0.08	-0.08

Table 2. FC structural and energetic parameters for H_2 adsorbed on Cu(111): the shortest distance between one H atom of the H_2 molecule and a substrate Cu atom, *d*, the H-H bond length, *l*, both in Å, the angle between the surface and the H_2 bond, α, in degrees, and the adsorption energies, E_{ads}, as calculated by PBE and PBE-D2 methods, both in eV.

3.1.2 *H_2 Adsorption on Cu(100)*

Similar to Cu(111) surface, six highly-symmetric H_2 adsorption geometries have been explored on the Cu(100) surface, see Figure 4, including top, bridge, and hollow sites. At variance with Cu(111), most of the conformations stay at the same position, maintaining the H_2 molecule parallel to the Copper surface, see structural values in Table 3. However, the adsorption energies at PBE computation level are already

significant, highlighting how the decrease in *nn* affects the chemical activity of surface Cu atoms. Indeed, the bridge 2b site is predominant over the other sites, although it is still a physisorption situation. Addition of vdW essentially doubles the attachment strength, but it still remains a physisorption, with an approaching of H_2 molecule to the surface of more than 1.3 Å. Besides, the adsorption on top of a Cu surface atom gets the molecular bond length slightly elongated by 0.03 Å plus the H_2 molecule is close to the Cu(100) surface, with Cu-H distances of ~2 Å. However, note that this is not the most stable site and H_2 molecules are unlikely to dissociate from this particular site, which would be just slightly populated to a Gibbs distribution (0.025%). Last, the adsorption on 2a site leads to a structure perpendicular to the Cu surface, in a similar fashion to the above commented cases on Cu(111) surface. Note that the adsorption energy is an order of magnitude larger than the values reported experimentally [40,41], however the adsorption energy and site allocation is in excellent agreement with a previous work using Embedded Atom Method (*EAM*) [42]. In that work both 1b and 2b sites were found to compete, with a slight preference for the 2b site, in terms of adsorption heat and dissociation energy barrier, and present and previous results do agree with other experimental values of the adsorption heat of ~ -0.42 to -0.52 eV [43].

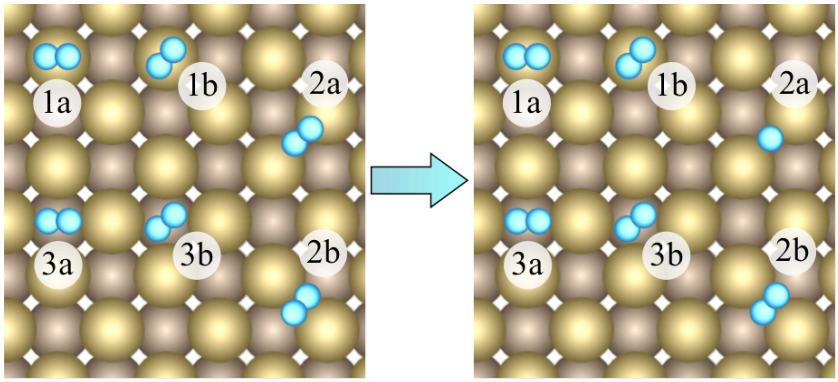

Figure 4. IC (left) and FC (right) for the sampled H_2 adsorption high-symmetry sites on Cu(100) surface. Atomic color-coding is as in Figure 3.

		1a	**1b**	**2a**	**2b**	**3a**	**3b**
PBE	***l* / Å**	0.78	0.78	0.75	0.75	0.75	0.75
	***d* / Å**	2.03	2.02	3.37	4.02	4.08	4.17

	α / º	0.1	0.4	87.0	0.0	0.0	0.0
	E_{ads} **/ eV**	-0.20	-0.21	-0.27	-0.42	-0.25	-0.25
PBE-D2	***l* / Å**	—	—	0.75	0.75	—	—
	***d* / Å**	—	—	2.04	2.64	—	—
	α / º	—	—	88.2	0.7	—	—
	E_{ads}^{vdW} **/ eV**	—	—	-0.68	-0.91	—	—

Table 3. FC structural and energetic parameters for H_2 adsorbed on Cu(100): the shortest distance between one H atom of the H_2 molecule and a substrate Cu atom, *d*, the H-H bond length, *l*, both in Å, the angle between the surface and the H_2 bond, α, in degrees, and the adsorption energies, E_{ads}, as calculated by PBE and PBE-D2 methods, both in eV.

3.1.3 *H_2 Adsorption on Cu(110)*

Here ten highly-symmetric adsorption geometries were sampled on the Cu(110) surface, including top, bridge, and hollow sites. Note that in this particular surfaces there are two kinds of bridge sites, the above commented sb (2a,b) and lb (2c,d) sites. Figure 5 shows ICs and FCs, and energetic and structural data are presented in Table 4. Here top adsorption sites with H_2 molecule oriented towards bridge sites are the most stable ones, in particular 1b, which points H atoms to sb sites, in agreement with previous studies determining sb sites to be the most stable for H adatoms [35]. Moreover, the H molecule gets its bond length increased by 0.04 Å, implying a bond weakening, and thus going for a dissociation. Last but not least, as happened with top sites on Cu(100) surface, the H_2 molecule gets close to the Cu(110) surface, with a Cu-H distance *d* of ~1.95 Å. The addition of a vdW description yields an increment of E_{ads} value similar to the Cu(100) surface, with negligible structure changes, with a lowering of the molecule of solely by ~0.1 Å in 1a and 1b cases, but of ~1 Å in the 2b case. It is noteworthy that the adsorption energy values are higher than for the Cu(111) surface, but smaller than the Cu(100) one, thus, against a trend governed by *nn*, contrary to the expected trend of adsorption strength decaying in the order Cu(110) > Cu(100) > Cu(111), as found for other adsorbates, such as hydrazine [29]. Apparently, H_2 adsorption disobeys the *nn* rule, and the particular Cu-H interaction, *i.e.* orbital

coupling, bias the adsorption strength, rather than the surface Cu saturation. Last, the site preference of 0.03 eV between 1a and 1b configurations is maintained when plugging vdW, but now with a somewhat more acute difference of 0.14 eV. Even more, the less energetic preference of 2b site is also maintained. Note that 2a and 2b displace to reach the 1a and 1b positions, although there H_2 molecule is located farther from the surface. In this sense, it appears that there are two minima of adsorption on each site, located at different heights, and possibly with a small energy barrier in between them. Thus, site preference seems to be properly described at PBE level even when differences are of a few hundreds of eV.

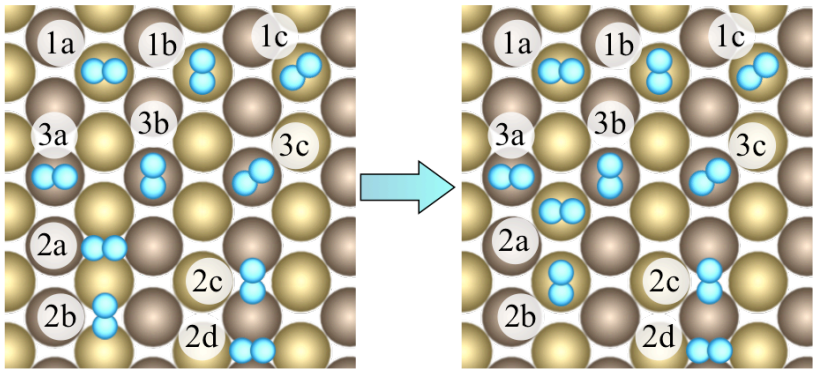

Figure 5. IC (left) and FC (right) for the sampled H_2 adsorption high-symmetry sites on Cu(110) surface. Note that positions 2a,b belong to sb sites, whereas positions 2c,d to lb sites. Atomic color-coding is as in Figure 3.

		1a	1b	1c	2a	2b	2c	2d	3a	3b	3c
PBE	***l* / Å**	0.78	0.79	0.75	0.75	0.75	0.75	0.75	0.75	0.75	0.75
	***d* / Å**	1.97	1.93	3.43	3.53	3.66	4.25	4.12	3.53	3.51	3.64
	α / º	0.0	0.0	0.0	0.0	1.0	0.0	0.0	0.8	1.5	0.3
	E_{ads} **/ eV**	-0.08	-0.11	-0.07	-0.07	-0.07	-0.06	-0.06	-0.07	-0.07	-0.07
PBE-D2	***l* / Å**	0.78	0.80	—	0.75	0.75	—	—	—	—	—
	***d* / Å**	1.89	1.84	—	2.50	2.62	—	—	—	—	—
	α / º	2.8	2.0	—	0.0	0.0	—	—	—	—	—
	E_{ads} **/ eV**	-0.65	-0.79	—	-0.51	-0.52	—	—	—	—	—

Table 4. FC structural and energetic parameters for H_2 adsorbed on Cu(110): the shortest distance between one H atom of the H_2 molecule and a substrate Cu atom, *d*, the H-H bond length, *l*, both in Å, the angle between the surface and the H_2 bond, α, in degrees, and the adsorption energies, E_{ads}, as calculated by PBE and PBE-D2 methods, both in eV.

3.1.4 *H_2 Adsorption on Cu Nanorows*

Last, we sampled four highly-symmetric adsorption geometries on the two Cu nanorows; *bottom-* and *top-displaced*. For this, H_2 molecules were placed at the nanorow apex, either on top or at bridge sites. Aside, they could be aligned with the nanorow direction, or perpendicular to it, see Figure 6. Results are encompassed in Table 5. Let us first focus on the *top-displaced* nanorow; here the adsorption energy values are rather low, of the same order to the Cu(110) surface, despite the *nn* is reduced to a value of 6, whereas Cu surface atoms on Cu(110) had a *nn* value of 7. Overall the H_2 molecule is placed parallel to the nanorow, and in some cases, like in position 1b, elongates by 0.05 Å. However, most stable adsorption site is 2a, where molecule rotates to adopt a perpendicular disposition with respect the Cu nanorow.

The addition of vdW forces, merely doubles the adsorption energy, which still remains rather low, at variance with Cu(110) surface, where the inclusion of a description of dispersive forces strengthened the interaction by almost 0.7 eV. This can be easily explained by the lack of Cu atoms in a close proximity to the hydrogen molecule, which makes that vdW interactions, which are additive in nature, and mostly raising from first neighbors, due to the rapid decay for more distant atoms, fall in very small contribution.

In the *bottom-displaced* case, the adsorption of H_2 is even weaker, and the molecule prefers to sit atop of the Cu apex nanorow atom. At variance with case 2a in *top-displaced*, here H_2 remains parallel to the nanorow, with an adsorption energy of -0.06 eV for both top 1a and 1b sites. Particularly, the 1a site features an elongated *l* H_2 bond length by 0.06 Å, which could be assimilated to the known Kubas adsorption mode found in organometallic compounds or supported metal adatoms [44,45]. Here the expected increase in the adsorption energy due to a reduced *nn* value of 5 is not observed, yet it can be explained in terms of the Kubas adsorption mode: the higher interaction with the Cu nanorow apex atom is counteracted by the energy necessary to elongate the H_2 bond. The addition of vdW, as above-explained, is mild.

All in all, the reduced *nn* of Cu nanorows does not necessarily imply a preferential adsorption of H_2, and indeed, H_2 would prefer to adsorb on the Cu (100) or (110) surfaces. On one hand, apparently the specific electronic arrangement in the nanorows does not match the H_2 molecular orbitals for a favorable interaction, on the other hand, the interaction of H_2 molecule may imply a bond distance elongation, which intrinsically demands an energetic cost, which goes in an opposite direction to the adsorption energy release.

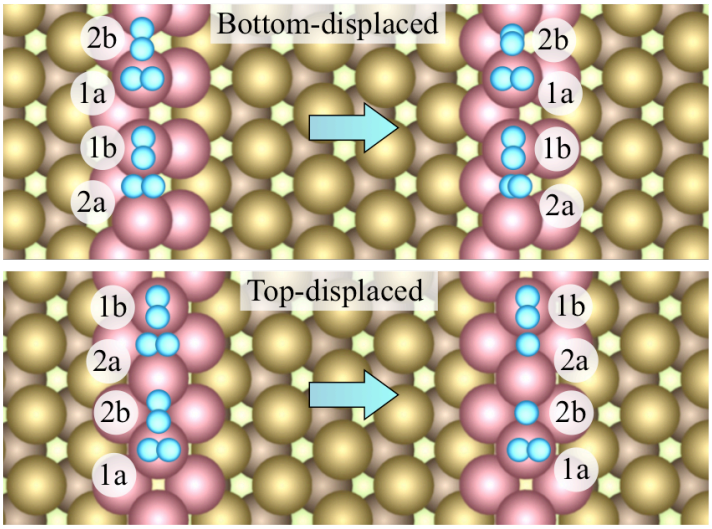

Figure 6. IC (left) and FC (right) for the sampled H_2 adsorption high-symmetry sites on Cu *bottom-* and *top-displaced* nanorows. Atomic color-coding is as in Figure 3.

		Top-displaced				**Bottom-displaced**			
		1a	**1b**	**2a**	**2b**	**1a**	**1b**	**2a**	**2b**
PBE	***l* / Å**	0.76	0.80	0.75	0.75	0.81	0.75	0.75	0.75
	***d* / Å**	2.20	1.84	4.02	3.34	1.84	2.59	2.55	2.60
	α / º	3.0	1.6	87.5	3.9	1.1	1.1	63.8	77.7
	E_{ads} / eV	-0.06	-0.05	-0.11	-0.04	-0.06	-0.06	-0.01	-0.01
PBE-D2	***l* / Å**	0.77	—	0.75	—	0.81	0.76	—	—

***d* / Å**	2.16	—	3.63	—	1.80	2.27	—	—
α / º	2.8	—	87.9	—	1.2	1.1	—	—
E_{ads} / eV	-0.11	—	-0.20	—	-0.15	-0.15	—	—

Table 5. FC structural and energetic parameters for H_2 adsorbed on Cu *Top*- and *Bottom-displaced* nanorows. the shortest distance between one H atom of the H_2 molecule and a substrate Cu atom, *d*, and the H-H bond length, *l*, are given in Å, the angle between the nanorow and the H_2 bond, α, in degrees. Adsorption energies, E_{ads}, as calculated by PBE and PBE-D2 methods, are given in eV.

3.2. H Adsorption

Here is explored the adsorption of two H atoms on the three Cu surfaces and the two nanorows, as explained in the computational details. FC are shown in Figure 7, and energetic and structural data are encompassed in Table 6, both for PBE and PBE-D2 calculations. As expected, H sits on four-fold hollow sites on Cu(100) surface, and *fcc* three-fold hollow sites on Cu(111) surface. Curiously, H atoms do like to sit on sb bridge sites on Cu(110) surface, but their stability is essentially isoenergetic as to have them on lb bridge sites, contrary to previous statements [35]. Probably the slight discrepancy with previous statements is due to small variations on the computational procedure or level, and being conservative one should consider both sites competitive. However, for the rest of the discussion we shall focus on lb sites. In the *top-displaced* nanorow case the H atoms remain on the three-fold hollow sites of adjacent nanorow facets, whereas in the case of *bottom-displaced* nanorow one H sits nearby the four-fold hollow site of the (100)-like facet, whereas the other one is more bridging two nanorow apex Cu atoms, see Figure 7.

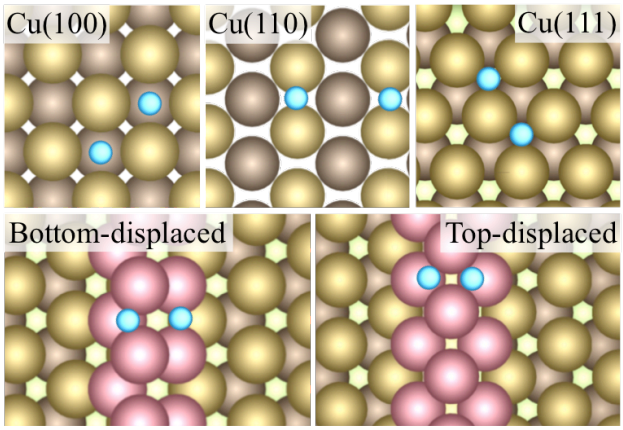

Figure 7. FC for two H adatoms on the different Cu surfaces and nanorows. Atomic color-coding is as in Figure 3.

	(111)	**(100)**	**(110)-sb**	**(110)-lb**	***Top-***	***Bottom-***
d / Å	1.76	1.91	1.30	1.83	1.64	1.87
E_{ads} / eV	-2.30	-2.53	-2.08	-2.11	-2.29	-2.43
d^{vdW} / Å	1.74	1.86	1.29	1.79	1.58	1.81
E_{ads}^{vdW} / eV	-2.38	-2.82	-2.24	-2.40	-2.53	-2.58

Table 6. FC structural and energetic parameters for 2 H adsorbed on Cu (111), (100), and (110) surfaces, and *Top-* and *Bottom-displaced* nanorows. Average distance between the H atoms and the surface plane or nanorow facet, d, are given in Å, for PBE and PBE-D2 (vdW superindex) calculations. Mean adsorption energies, E_{ads}, are given in eV for the nanorow case.

In general terms H atoms in any of the surfaces or nanorows is strongly attached and so chemisorbed, with E_{ads} values below -2 eV. In relation with that, such H atoms are located close to the Cu surface, typically in between 1.5-2 Å, yet in some cases, like in bridge sites of Cu(110) surface, such small H atoms can even sink placing themselves almost in plane with the Cu surface. There is apparently no clear change in the adsorption strength depending on the coordination *nn* values, as happened with H_2 molecule adsorption. The addition of vdW implies in all cases a small reduction of the adsorption energies ranging 0.1-0.3 eV, and so, dispersive forces are not the main contribution in such interactions, at variance with H_2 molecule. Because of this, addition

of vdW seems to be mandatory when treating not only H_2 adsorption on Cu surfaces, but also its dissociation, given that they are the main force in the initial state, and probably playing an effect in the dissociation transition states.

3.3. Trends in H_2 Adsorption and Dissociation

Here the trends in the adsorptive and dissociated states of H_2 on the different Cu surfaces and nanorows are put under light, as well as the dissociation process. Table 7 summarizes the adsorption energy values obtained both at PBE and PBE-D2 calculation levels, as commented in the previous sections, plus the H_2 dissociation energy on the substrate, ΔE_r, defined as:

$$\Delta E_r = 2 \cdot E_{ads}^{H} - E_{diss}^{H_2} - E_{ads}^{H_2} \quad (5),$$

where E_{ads}^{H} and $E_{ads}^{H_2}$ are the adsorption energies of H atom and H_2 molecule, respectively, and $E_{diss}^{H_2}$ is the dissociation energy of H_2 molecule in vacuum, defined as:

$$E_{diss}^{H_2} = E_{H_2} - 2 \cdot E_H \quad (6),$$

where E_{H_2} is the total energy of a H_2 molecule in vacuum, and E_H that of a H atom in vacuum, obtained as explained in the computational details section. Either at PBE or PBE-D2 computational levels, $E_{diss}^{H_2}$ is found to be 4.53 eV. Note that this atypical definition of ΔE_r is equivalent to:

$$\Delta E_r = E_{2 \cdot H/surf} - E_{H_2/surf} \quad (7),$$

this is, the difference in energy with the Cu-substrate with H_2 molecule or 2 H atoms adsorbed, $E_{2 \cdot H/surf}$ and $E_{H_2/surf}$, respectively. Table 7 also encompasses the obtained energy barriers E_{barr}, as detailed in the computational details. Note that the TS reported, obtained at the PBE-D2 level, are characterized as saddle points by a frequency analysis finding a sole imaginary frequency.

	(111)	**(100)**	**(110)**	***Top-***	***Bottom-***
nn	9	8	7	6	5

PBE	$E_{ads}^{H_2}$	-0.002	-0.42	-0.11	-0.11	-0.06
	E_{ads}^{H}	-2.30	-2.53	-2.11	-2.29	-2.43
	ΔE_r	-0.07	-0.11	0.42	0.06	0.27
PBE-D2	$E_{ads}^{H_2}$	-0.08	-0.91	-0.79	-0.20	-0.15
	E_{ads}^{H}	-2.38	-2.82	-2.40	-2.53	-2.58
	ΔE_r	-0.15	-0.20	0.52	-0.33	-0.48
	E_{barr}	0.55	0.12	0.53	0.53	0.59

Table 7. Adsorption energies for H_2 and H, $E_{ads}^{H_2}$ and E_{ads}^{H}, respectively, as well as the H2 dissociation exothermicity, ΔE_r, all values in eV, obtained at PBE and PBE-D2 computational levels, for Cu (111), (100), and (110) surfaces, and *Top*- and *Bottom-displaced* nanorows. Nearest-neighbor values, *nn*, are also displayed.

The values in Table 7 can be plotted against *nn*, see Figure 8, and many conclusions can be withdrawn. First, the adsorption energy of H_2, as calculated by PBE level, does not lower with respect *nn*. Indeed, a maximum interaction is found for Cu(100). The addition of vdW description, yet important, does not alter the situation for Cu(111) surface and Cu nanorows, yet implies a high strengthening of the interaction in the cases of Cu (100) and (110) surfaces. As far as the adsorption energy of H adatoms is concerned, Figure 8 shows that the binding strengthening as a function of a *nn* reduction is observed just in some parts, and indeed the *nn* variation for the low-index Miller surfaces studied does not imply a clear patterned change in the adsorption energy, specially disrupted for the Cu (100) and (111) surfaces. The addition of vdW forces description lowers the adsorption energy values for all the studied cases essentially the same, with very little effect on the overall trend.

Last, we inspected the reaction exothermicity in terms of ΔE_r values. PBE generates some results that should be treated with caveats. In the case of Cu(111) surface, the H_2 dissociation is found to be thermodynamically favoured, yet the very small H_2 adsorption energy prompts to think that H_2 would desorb before dissociating. Indeed, by inspecting the E_{barr} values in Table 7, that is what it would happen, given that the energy barrier of 0.55 eV is an order of magnitude higher than the desorption energy. Almost the same degree of exothermicity is found for Cu(100) surface, yet here

the H_2 adsorption energy is higher, and so, this surface would be more likely to capture and dissociate H_2 than Cu(111). This is supported by a small dissociation energy barrier of 0.12 eV, making the dissociation much more viable than the H_2 desorption. Note that despite the H_2 adsorption energy and site match previous simulations [42], present energy barrier is sensibly lower than previous reported values 0.51-0.58 eV [42,46], but however in more accordance with reported values of ~0.2 eV as reported in the literature [47]. Considering the Cu(110) surface, yet having a reduced *nn*, it does not imply a stronger adsorption of H_2, nor a stronger adsorption of H adatoms as well. Consequently, H_2 dissociation is unlikely to happen in such a surface, given the pronounced endothermicity, despite such a surface could be equally represented in a Cu nanoparticle, following the surface stability values reported in Table 1. The energy barrier for this surface is 0.50 eV, in agreement with a reported experimental value of 0.62 ± 0.06 eV [48].

Similarly yet unexpectedly, H_2 dissociation seems to be unlikely on low-saturated sites, as found for Cu nanorows. Indeed, the H_2 adsorption is not specially high, similar to Cu(110), plus the H adatoms are not remarkably stable. The consequence is that here, as well, H_2 dissociation is an endothermic process, and so, unlikely to happen in standard conditions. Following this argument, one would be prompted to claim that low-coordinated sites on Cu nanoparticles are not playing any key role in H_2 dissociation, a statement that is surprising, knowing how low-coordinated sites are typically implying a higher activity, as found in many previous studies [13,49,50]. This leads to think that H_2 dissociation is less favoured whenever less surface coordination is.

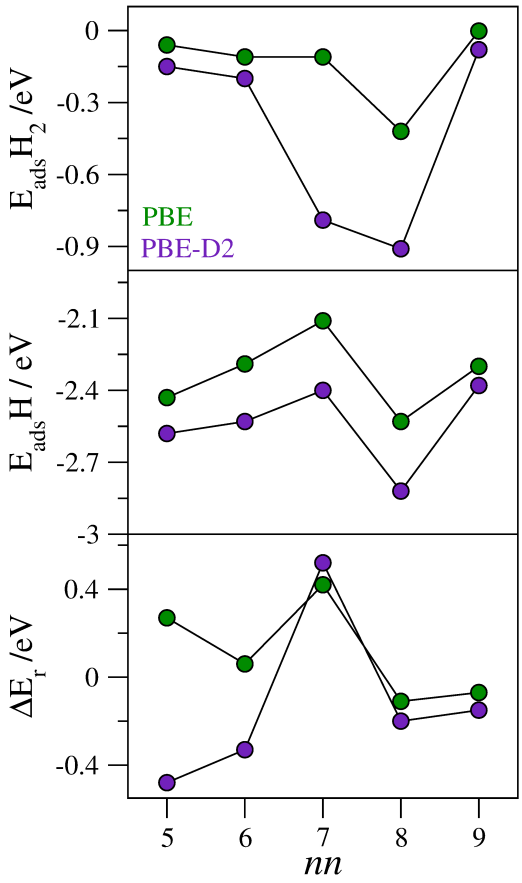

Figure 8. Most stables adsorption energies of H_2 molecule (top panel), and of an H atom (middle panel), and H_2 dissociation exothermicity (bottom panel) *versus* the nearest-neighbors number, *nn*.

However this picture may be changed when vdW interactions are properly described. In this sense, as seen in Figure 8, the change by adding dispersive forces is little for Cu surfaces. Indeed, the exothermicity related to surface H_2 dissociation increases a little in the case of Cu(111) and Cu(100) surfaces, yet it is slightly detrimental in the special case of Cu(110) surface. However, a large change is observed for the low-coordinated sites of Cu nanorows. Here H_2 dissociation process changes from clearly endothermic to clearly exothermic, in essence due to the highest stabilization of H adatoms compared to that of H_2 molecules by vdW forces. Therefore, H_2 molecules can physisorb on these sites, plus their dissociation is favoured, more than in any other regular defect-free surfaces. Last but not least, with the caveat of Cu(110) surface, the ΔE_r values show a nice linear trend with respect *nn*, given that vdW forces are accounted for.

Some previous and recent studies highlighted the linear relationship in between on adsorbate and another adsorbate adsorption energies, obtained for species attaching by a main group element (C, N, O, or S) atom [51], which recently has been found to be influenced by *nn* [52]. Note that such a relationship in between H_2 and H adsorption energies, and ΔE_r with respect these two yielded no linear trend (not shown). This highlights that H seems to be a very peculiar system which disobeys previous found trends, being an exception to the rule, and so must be treated with care and caution.

Already at the PBE-D2 level one could try to obtain the known Brønsted-Evans-Polanyi (BEP) relationship [53-55], which linearly relate the observed activation energy, E_{act}, of a reaction or elementary step, and the reaction energy, ΔE, here defined as:

$$E_{act} = E_{TS/surf} - E_{H_2} - E_{surf} \quad (8),$$

$$\Delta E = E_{2\cdot H/surf} - E_{H_2} - E_{surf} \quad (9).$$

Such quantities have been evaluated from data contained in Table 7, and the BEP relationship is shown in Figure 9. From its inspection it is apparent the overall trend, this is, the larger the exothermicity, the lower the barrier. However, a linear trend is not observed ($R^2 < 0.35$), and so, H_2 dissociation on Cu systems seems to be an outlier of the general BEP relationships as found on metals, oxides, and carbides [54]. Note that considering that the E_{barr} is similar for all the studied substrates and equal to ~0.55 eV —with the caveat of Cu(100) surface—, one would think that such process is equally likely on all the surfaces, but here thermodynamics do play a key role. For instance, on Cu(111) surface and Cu nanorows the H_2 dissociation, despite being exothermic, features a TS above the reagent energy level, and so energy should be supplied to overcome it. On the contrary, for Cu(110) and Cu(100) surfaces, the TS is located below the reagent energy level, and so part of the energy of H_2 adsorption could be utilized, when no dispersed on the Cu surface, to overcome the energy barrier. Particularly, Cu(100) surfaces or facets are highlighted as the main character in H_2 dissociation.

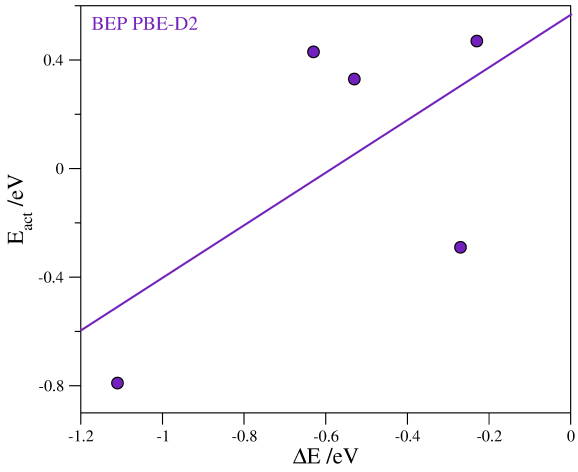

Figure 9. BEP relationship as calculated at PBE-D2 level for H_2 dissociation on Cu (100), (110), and (111) surfaces, and *Top*- and *Bottom-displaced* Cu nanorows.

4. Conclusions

Here we presented a thorough density functional theory study, including and excluding dispersive forces interaction description, on the adsorption and dissociation of H_2 molecule on the low-index Miller Cu (111), (100), and (110) surfaces, displaying a reducing number of surface nearest-neighbours, *nn*, as a measurement of the saturation degree, as well as on two different surface Cu nanorows deposited on Cu(111) surface. The computational setup has been optimized granting an accuracy below 0.04 eV. Most stable adsorption sites and geometries are delivered.

Surface and nanorow energies —for the latest a new methodology to extract the is presented— are found to follow the *nn* number. The most stable substrates are thought to attach H_2 stronger, yet this is statement is found to be unaccomplished, and this is also found for the optimized H adatoms situation obtained from a H_2 molecule dissociation. The adsorption strengths seem to be governed by a particular orbital↔ band interaction rather than by the simple *nn* coordination. Furthermore, despite overall Brønsted-Evans-Polanyi trend is followed, the linear relationship is absent, making H_2 dissociation on Cu surfaces an outlier of the general trends found on metals, oxides, and carbides. Aside, vdW forces are found to play a key role in the adsorption of H_2, and merely an energetic adjustment on chemisorbed H adatoms.

No clear trends are observed for the evolution of H_2 and H adsorption energies, as well as the H_2 dissociation energy with respect *nn*, and among theses quantities, making H_2 adsorption and dissociation a trend outlier compared to other molecules and

processes. Indeed, it is found that H_2 is likely to dissociate on Cu(100) surface given a significant H_2 molecule adsorption energy and being the process slightly exothermic, with a very small energy barrier of 0.12 eV. On the Cu(111) surface the rather smaller H_2 adsorption energy would prevent H_2 dissociation, regardless is thermodynamically driven to, added to the fact that the dissociation energy barrier is of 0.55 eV. On Cu(110) surface H_2 molecules are likely to attach, but the dissociation process is markedly endothermic with a sensibly large energy barrier of 0.53 eV. For the low-coordinated sites on Cu nanorows, vdW interactions inclusion play a key role in order to investigate the H_2 dissociation process, which otherwise is found to be endothermic, and so, unlikely. However, dispersive forces turn the process markedly exothermic, making it viable, yet the dissociation energy barriers are ~0.55 eV. Consequently, a nanoparticle Cu system must preferably display Cu(100) surfaces or facets in order to dissociate H_2, vital in many hydrogenation processes. Finally, note that dispersive forces description results mandatory in treating such processes.

5. References

[1] K. Liu, C. Song, V. Subramani, Hydrogen and Syngas Production and Purification Technologies, Wiley and AlChE, Canada, 2010.

[2] L. Gradisher, B. Dutcher, M. Fan, Appl. Energ. 139 (2015) 335.

[3] S.T. Yong, C.W. Ooi, S.P. Chai, X.S. Wu. Int. J. Hydrogen Ener. 38 (2013) 9541.

[4] T. Tsoncheva, I. Genova, M. Dimitrov. E. Sarcadi-Priboczki, A.M. Venezia, D. Kovacheva. N. Scotti, V. dal Santo, Appl. Catal B-Environ. 165 (2015) 599.

[5] R. Pérez-Hernández, G.M. Galicia, D.M. Anaya, J. Palacios, C. Angeles-Chavez, J. Arenas-Alatorre. Int. J. Hydrogen Ener. 33 (2008) 4569.

[6] J.A. Rodriguez, P. Liu, X. Wang, W. Wen, J. Hanson, J. Hrbek, M. Peréz, J. Evans, Cat. Today 143 (2009) 45.

[7] G. Cilpa, G. Chambaud, Surf. Sci. 601 (2007) 320.

[8] J.R. Álvarez-Collado, Surf. Sci. 600 (2006) 133.

[9] M. Bonfanti, C. Díaz, M.F. Somers, G.J. Kroes, Phys. Chem. Chem. Phys. 13 (2011) 4552.

[10] Z. Wang, X. Liu, D.W. Rooney, P. Hu, Surf. Sci. (2015), DOI: 10.1016/j.susc.2015.01.004.

[11] B. Hammer, M. Scheffler, K.W. Jacobsen, J.K. Nørskov, Phys. Rev. Lett. 73 (1994) 1400.

[12] J. Radilla, M. Boronat, A. Corma, F. Illas, Phys. Chem. Chem. Phys. 12 (2010) 6492.

[13] F. Viñes, J.R.B. Gomes, F. Illas, Chem. Soc. Rev. 43 (2014) 4922.

[14] F. Viñes, A. Görling. Angew. Chem. Int. Ed. 50 (2011) 4611.

[15] S. Sakong, A. Groß, Surf. Sci. 525 (2003) 107.

[16] J.P. Perdew, K. Burke, M. Ernzerhof, Phys. Rev. Lett. 77 (1996) 3865.

[17] P. Janthon, S. Luo, S.M. Kozlov, F. Viñes, J. Limtrakul, D.G. Truhlar, F. Illas, J. Chem. Theory Comput. 10 (2014) 3832.

[18] G. Kresse, J. Furthmüller, Phys. Rev. B 54 (1996) 11169.

[19] G. Kresse, J. Hafner, Phys. Rev. B 47 (1993) 558.

[20] P. Blöchl, Phys. Rev. B 50 (1994) 17953.

[21] H.J. Monkhorst, J.D. Pack, Phys. Rev. B 13 (1976) 5188.

[22] P. Janthon, S.M. Kozlov, F. Viñes, J. Limtrakul, F. Illas, J. Chem. Theory Comput. 9 (2013) 1631.

[23] F. Viñes, C. Sousa, P. Liu, J.A. Rodriguez, F. Illas, J. Chem. Phys. 122 (2005) 174709.

[24] S. González, F. Viñes, J.F. García, Y. Erazo, F. Illas, Surf. Sci. 625 (2014) 64.

[25] A. Corma, M. Boronat, S. González, F. Illas, Chem. Commun. 2007, 3371.

[26] A. Roldán, S. González, J.M. Ricart, F. Illas, ChemPhysChem 10 (2009) 348.

[27] S.M. Kozlov, F. Viñes, N. Nilius, S. Shaikhutdinov, K.M. Neyman, J. Phys. Chem. Lett. 3 (2012) 1956.

[28] S. Grimme, J. Comp. Chem. 115 (2001) 8748.

[29] S.S. Tafreshi, A. Roldán, N.H. de Leeuw, J. Phys. Chem. C 118 (2014) 26103.

[30] P. Janthon, F. Viñes, S.M. Kozlov, J. Limtrakul, F. Illas, J. Chem. Phys. 138 (2013) 244701.

[31] S. Grimme, J. Antony, S. Ehrlich, H. Krieg, J. Chem. Phys. 132 (2010) 154104.

[32] J. Gebhardt, F. Viñes, P. Bleiziffer, W. Hieringer, A. Görling, Phys. Chem. Chem. Phys. 16 (2014) 5382.

[33] K. Mudiyanselage, Y. Yang, F.M. Hoffmann, O.J. Furlong, J. Hrbek, M.G. White, P. Liu, D.J. Stacchiola, J. Chem. Phys. 139 (2013) 044712.

[34] A.P. Graham, D. Fang, E.M. McCash, W. Allison, Phys. Rev. B 57 (1998) 13158.

[35] X.-Y. Pang, L.-Q. Xue, G.-C. Wang, Langmuir 23 (2007) 4910.

[36] R.F. Bader, Atoms in Molecules: A Quantum Theory, Oxford Science, Oxford, U.K. 1990.

[37] G. Henkelman, H. Jónsson, J. Chem. Phys. 111 (1999) 7010.

[38] K. Li, C. He, M Jiao, Y. Wang, Z. Wu, Carbon 74 (2014) 255.

[39] Z. Jiang, P. Qin, T. Fang, Chem. Phys. 445 (2014) 59.

[40] S. Andersson, L. Wilzén, M. Persson, Phys. Rev. B 38 (1988) 2967.

[41] J. Perrau, J. Laupjoulade, Surf. Sci. 121 (1982) 341.

[42] X. Jianjun, J. Ping, Z. Kaiming, J. Phys.: Condens. Matter 6 (1994) 7217.

[43] C.S. Alexander, J. Pritchard, J. Chem. Soc., Faraday Trans. 1 (1972) 202.

[44] G.J. Kubas, R.R. Ryan, B.I. Swanson, P.J. Vergamini, H.J. Wasserman, J. Am. Chem. Soc. 106 (1984) 451.

[45] H. Valencia, A. Gil, G. Frapper, J. Phys. Chem. C 119 (2015) 5506.

[46] P.B. Rasmussen, P.M. Holmblad, H. Christoffersen, P.A. Taylor, I. Chorkendorff, Surf. Sci. 287 (1993) 79.

[47] G. Anger, A. Winkler, K.D. Rendulic, Surf. Sci. 220 (1989) 1.

[48] J.M. Campbell, C.T. Campbell, Surf. Sci. 259 (1991) 1.

[49] F. Viñes, Y. Lykhach, T. Staudt, M.P.A. Lorenz, C. Papp, H.-P. Steinrück, J. Libuda, K.M. Neyman, A. Görling, Chem. Eur. J. 16 (2010) 6530

[50] N. Luckas, F. Viñes, M. Happel, A. Desikusumastuti, J. Libuda, A. Görling, J. Phys. Chem. C 114 (2010) 13813.

[51] F. Abild-Pedersen, J. Greeley, F. Studt, J. Rossmeisl, T.R. Munter, P.G. Moses, E. Skúlason, T. Bligaard, J.K. Nørskov, Phys. Rev. Lett. 99 (2007) 016105.

[52] F. Calle-Vallejo, D. Loffreda, M.T.M. Koper, P. Sautet, Nature Chem. 7 (2015) 403.

[53] M.G. Evans, M. Polanyi, Trans. Faraday Soc. 34 (1938) 11.

[54] F. Viñes, A. Vojvodic, F. Abild-Pedersen, F. Illas, J. Phys. Chem. C 117 (2013) 4168.

[55] J.N. Brønsted, Chem. Rev. 5 (1928) 231.